UNIVERSITY *of York*

This is a repository copy of *Target Deformation of the Equus stenonis Holotype Skull:A Virtual Reconstruction*.

White Rose Research Online URL for this paper:
https://eprints.whiterose.ac.uk/id/eprint/163957/

Version: Published Version

Article:

Cirilli, Omar, Melchionna, Marina, Serio, Carmela et al. (6 more authors) (2020) Target Deformation of the Equus stenonis Holotype Skull:A Virtual Reconstruction. Frontiers in Earth Science. 247. ISSN: 2296-6463

https://doi.org/10.3389/feart.2020.00247

White Rose
university consortium
Universities of Leeds, Sheffield & York

eprints@whiterose.ac.uk
https://eprints.whiterose.ac.uk/

Target Deformation of the *Equus stenonis* Holotype Skull: A Virtual Reconstruction

Omar Cirilli[1,2]*, Marina Melchionna[3], Carmela Serio[4], Raymond L. Bernor[5,6], Maia Bukhsianidze[7], David Lordkipanidze[7], Lorenzo Rook[2], Antonio Profico[8] and Pasquale Raia[3]

[1] Dottorato di Ricerca in Scienze della Terra, Università degli Studi di Pisa, Pisa, Italy, [2] Paleo[Fab]Lab, Dipartimento di Scienze della Terra, Università degli Studi di Firenze, Firenze, Italy, [3] Dipartimento di Scienze della Terra, dell'Ambiente e delle Risorse, Università degli Studi di Napoli Federico II, Naples, Italy, [4] Research Centre in Evolutionary Anthropology and Palaeoecology, School of Biological and Environmental Sciences, Liverpool John Moores University, Liverpool, United Kingdom, [5] Laboratory of Evolutionary Biology, Department of Anatomy, College of Medicine, Howard University, Washington, DC, United States, [6] Human Origins Program, Department of Anthropology, National Museum of Natural History, Smithsonian Institution, Washington, DC, United States, [7] Georgian National Museum, Tbilisi, Georgia, [8] PalaeoHub, Department of Archaeology, University of York, Heslington, United Kingdom

Equus stenonis is one of the most prevalent European Pleistocene fossil horses. It is believed to be the possible ancestor of all Old World Early Pleistocene *Equus*, extant zebras and asses, and as such provides insights into *Equus* evolution and its biogeography and paleoecology. The *Equus stenonis* holotype skull (IGF560) was first described by Igino Cocchi in 1867, from the Early Pleistocene locality of Terranuova (Upper Valdarno basin, Italy). IGF560 is a nearly complete, although medio-laterally crushed and badly compressed skull. Here we provide the first application of a new virtual reconstruction protocol, termed Target Deformation, to the *Equus stenonis* holotype. The protocol extends beyond classic retrodeformation by using target specimens as a guide for the virtual reconstruction. The targets used as a reference are two fragmentary, yet well-preserved *E. stenonis* skulls, coming from Olivola (Italy; IGF11023) and Dmanisi (Georgia; Dm 5/154.3/4.A4.5), both Early Pleistocene in age. These two specimens do not display any major deformation, but preserve different, only slightly overlapping portions of the skull. The virtual reconstruction protocol we carried out has shown its feasibility, by producing two 3D models whose final morphology is perfectly congruent with the natural variability of a comparative sample of *E. stenonis* specimens. This study shows the potential of using even broken or otherwise fragmentary specimens to guide retrodeformation in badly distorted and damaged specimens. The application of Target Deformation will allow us to increase the availability of comparative specimens in studies of fossil species morphology and evolution, as well as to the study of taphonomic processes.

Keywords: *Equus stenonis*, target deformation, virtual reconstruction, 3D, equidae

INTRODUCTION

A number of taphonomic processes are known to alter the physical preservation of fossil remains. As a consequence, fossils usually become badly deformed (e.g., losing biological symmetry, being compressed or bent) or incomplete (Shipman, 1981; Lyman, 1994; Schlager et al., 2018). The lack of this valuable information worsens the already fragmentary fossil record, which limits the opportunity to study fossil remains with the same analytical power that is typical for neontological samples. Therefore, paleontologists have to face the classic challenge to take the best out of specimens which show significant deformations, miss anatomical parts, or both. Remains of fossil horses provide no exception. Although moderately frequent in the fossil record, horses are mostly represented (and studied) by post-cranial elements, which by virtue of their stocky built (in the case of long bones) and low aspect ratio (in the case of legs distal elements) are much less deformed (or broken) than either mandibles or skulls. The latter are elongated and full of complex intracranial and extracranial cavities in horses, which makes their complete, undistorted preservation potential exceedingly low (Budras et al., 2009).

Herein, we present a new virtual reconstruction protocol, termed Target Deformation, which takes advantage of recent progress in digital restoration of fossil specimens, including retrodeformation (Schlager et al., 2018), digital alignment of disarticulated portions (DTA, Profico et al., 2019b), and 3D thin plate spline transformation (tps3d) (Bookstein, 1989; Schlager et al., 2018) to provide the virtual reconstruction of badly deformed, partially incomplete cranial material by using target fossil remains of the same species. We demonstrate here that our procedure is viable even by using very incomplete target remains, which are common in the fossil record and cannot be used by themselves in comparative analyses.

Our case study is the *Equus stenonis* holotype skull (IGF560, **Figure 1**), originating from the Early Pleistocene locality of Terranuova (Tuscany, Italy), is a 1.8 Ma locality in the Upper Valdarno Basin, which is housed in the Natural History Museum (Geology and Paleontology Section) of the University of Florence. We applied Target Deformation to the *E. stenonis* holotype by using two different targets, an incomplete *E. stenonis* skull (Dm 5/154.3/4.A4.5; **Figure 2**) originating from Dmanisi,

Georgia, and another partial skull (IGF11023; **Figure 3**) retrieved from the fossil locality of Olivola, Italy. Both target skulls are lacking large portions of their crania. Importantly, the Dmanisi specimen has a nicely undeformed mid-cranial vault entirely lacking the muzzle. In contrast, the Olivola skull neurocranium is missing most of the cranial vault, while preserving the muzzle.

The virtual reconstruction carried out herein has demonstrated the feasibility of this method, by the production of two 3D models whose final morphology is fully congruent with a comparative sample of *E. stenonis* specimens from other localities in Europe. Eventually, by reflecting the right side of the 3D *E. stenonis* holotype model, we produced a fully symmetrical, vivid representation of the original skull shape in the *Equus stenonis* holotype specimen.

Equus stenonis

Equus stenonis Cocchi, 1867 (**Figure 1**) is the most common Early Pleistocene European fossil horse. It occurs in Spanish, French, Italian, Bulgarian, Romanian, and Greek Early Pleistocene localities (Alberdi et al., 1998; Athanassiou, 2001; Azzaroli, 2003; Alberdi and Palombo, 2013; Bernor et al., 2019; Boulbes and van Asperen, 2019), and in the Georgian locality of Dmanisi (Vekua, 1995) even if its chronological range still remains undefined. Nomade et al. (2014), assigned a new 2.4 Ma age to the French locality of Saint Vallier, yielding *Equus stenonis vireti* Prat (1964) which therefore represents the oldest evidence of this species in Europe. *Equus stenonis* last occurrence is more debatable, although the horse's presence at Farneta/Pirro Nord Faunal Units (FU), in Italy, correlated to circa 1.5–1.3 Ma, possibly represents the species last appearance being replaced shortly thereafter by *Equus suessenbornesis* (Alberdi and Palombo, 2013; Palombo and Alberdi, 2017).

The *Equus stenonis* holotype is a skull with associated mandible (IGF560), discovered by the Italian paleontologist Igino Cocchi in the 1867 near Terranuova (Arezzo, Tuscany), a 1.8 Ma fossil locality in the Upper Valdarno basin in Central Italy, belonging to the Olivola/Tasso Faunal Unit (FU). The skull is housed in the Natural History Museum in Florence. Cocchi named the species, without any description. A preliminary
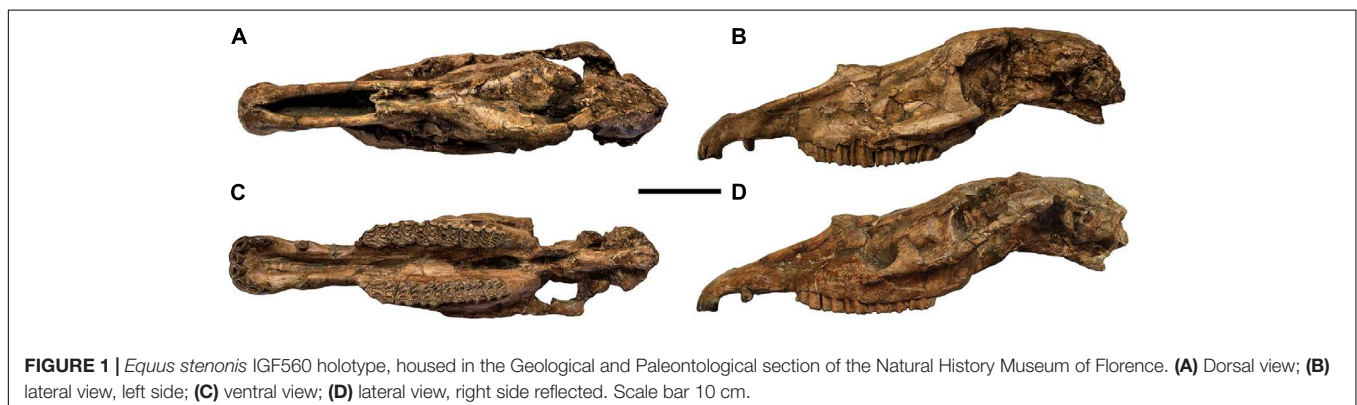

FIGURE 1 | *Equus stenonis* IGF560 holotype, housed in the Geological and Paleontological section of the Natural History Museum of Florence. **(A)** Dorsal view; **(B)** lateral view, left side; **(C)** ventral view; **(D)** lateral view, right side reflected. Scale bar 10 cm.
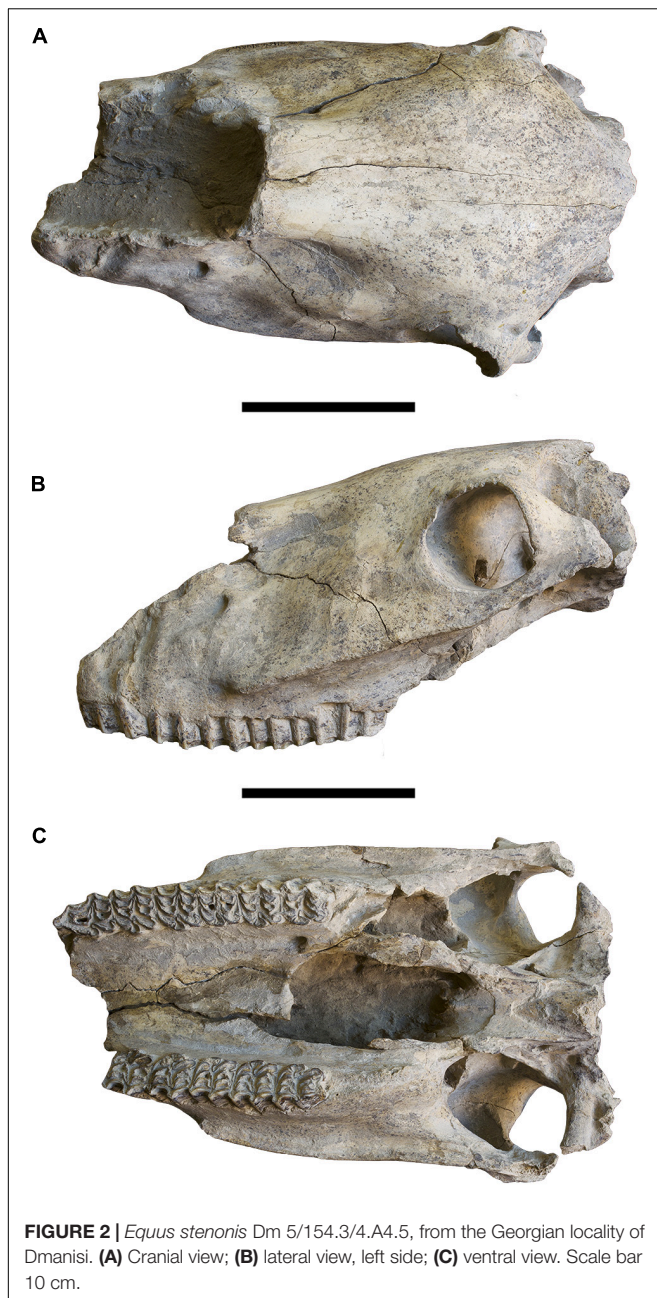
FIGURE 2 | *Equus stenonis* Dm 5/154.3/4.A4.5, from the Georgian locality of Dmanisi. **(A)** Cranial view; **(B)** lateral view, left side; **(C)** ventral view. Scale bar 10 cm.

description was later given by Forsyth Major (1885) and, in more detail, by Azzaroli (1964). De Giuli (1972) wrote a comprehensive review of the anatomical features of the *E. stenonis* sample from Olivola. *Equus stenonis* was discussed in several papers during the last few years, focusing on its biogeographic dispersion and its phylogenetic position within the stenonine horse group (Alberdi et al., 1998; Forsten, 1999; Athanassiou, 2001; Azzaroli, 2003; Alberdi and Palombo, 2013; Palombo et al., 2017; Boulbes and van Asperen, 2019). Recently, Bernor et al. (2019) provided an updated description of the holotype, demonstrating its relationships with the Old World

Equus and extant zebras and its possible relationship with the North American *Equus simplicidens*.

Equus stenonis Holotype Skull IGF560

The *Equus stenonis* holotype is an almost complete, medio-laterally deformed skull, lacking its left zygomatic arch. The skull has an elongated snout with a large canine, indicating that it is an adult male. The nasal bones are retracted to the level of P3 mesostyle. The snout is elongate with an arcuate incisor arcade. The maxillary cheek teeth are inclusive of dP^1-M^3. The M^3 is worn, dP^1 is (remarkably) still in place although with advanced wearing. The maxillary cheek teeth have the following features: dP^1 is small and rounded; P^2 has a short anterostyle; all cheek teeth have a short protocone linked to the protoloph; pli caballins are single on all cheek teeth; fossettes are well developed on P^2-P^4 and M^2, lesser developed on M^1 and M^3; hypoglyph is moderately deep on P^2-M^2 and not expressed on M^3.

In ventral view, the palatine processes of the muzzle are medio-laterally compressed, but the muzzle breadth between the posterior I^3 borders is well preserved. The palate is highly compressed, and the left upper teeth row is rotated counterclockwise to the internal side and slightly sheared in its antero-posterior sagittal plane. The choanae are heavily distorted and medio-laterally compressed, even if the vomer and the basisphenoid bones are preserved. The ventral occipital bones are damaged, yet the paracondylar processes within the occipital condyles and the foramen magnum are preserved.

In lateral view, the preorbital fossa is faintly delimited as a depression on the postero-superior maxilla level, and the facial maxillary crest is strongly developed on both sides. The zygomatic bone is preserved on the right side only. The orbits are preserved on the right side, while only the anterior ridge of the left orbit is present. The skull shows significant damage in the lateral maxillary region and the area of the paranasal sinuses, being more evident on the right side with respect to the nasal bones. The rostral process is not preserved.

In dorsal view, the temporal bones are preserved on both sides, although compressed medio-laterally. The right frontal bone above the orbital process. On the left side the frontal bone is strongly compressed with concomitant plastic deformation of the frontal sinuses and a shear compression along the sagittal plane. The maxillary and premaxillary bones (the muzzle) are well preserved, although the latter shows a slight counterclockwise rotation on the left side, as it is apparent in the positioning of the left P^2-M^3 cheek teeth row.

Equus stenonis Dm 5/154.3/4.A4.5, Dmanisi

The Dmanisi *Equus stenonis* fossil specimen Dm 5/154.3/4.A4.5 (**Figure 2**) was used as a retrodeformation target. The skull is lacking the muzzle and the occipital bones, although the cranial vault is complete and undeformed. The skull shows the typical *E. stenonis* occlusal maxillary cheek tooth pattern, including presence of short, squared protocones connected to the protoloph, which is a characteristic of the *E. stenonis* holotype.

In ventral view, the maxillary cheek tooth rows are nearly complete (only the right P[2] is missing) and the teeth show a medium stage of wear. The palate and the choanae are well preserved, the pterygoid bones are lacking, but the anterior border of the vomer is preserved. The two mandibular fossa of the zygomatic process are preserved.

In lateral view, the skull does not display any deformation. The preorbital fossa is small but clearly visible, and dorsally placed on both sides. The infraorbital foramen is preserved on the left side, the two facial maxillary crests are strongly developed from the zygomatic process up to P[4]/M[1] vertical border in both sides and are clearly distinguishable from the orbital processes. The two maxillae do not show any deformation in correspondence to the paranasal sinus.

In dorsal view, the occipital bones are missing, and the frontal bones do not show any deformation in correspondence to the frontal sinuses. The supraorbital foramina are preserved. The nasal bones are broken but preserved up to the level of the preorbital fossa.

Equus stenonis IGF11023, Olivola

The *Equus stenonis* specimen from Olivola (**Figure 3**) is our second target skull. The skull is incomplete having preserved its muzzle and palatal regions. The skull, although damaged on the lateral and dorsal surfaces, does not show any sign of deformation in ventral view. The palatine process is preserved in the premaxilla with all the upper incisors *in situ*, except for the right I1. The palate is not deformed although the choanae are missing. The two maxillary tooth rows are well preserved, the teeth are in a middle stage-of-wear. The protocone displays the typical *E. stenonis* morphology. In lateral view, the two facial maxillary crests are well developed up to the P[4]/M[1] boundary on both sides. The zygomatic processes are not preserved, the left orbital process is present. The skull shows a slight deformation in proximity to the paranasal sinuses.
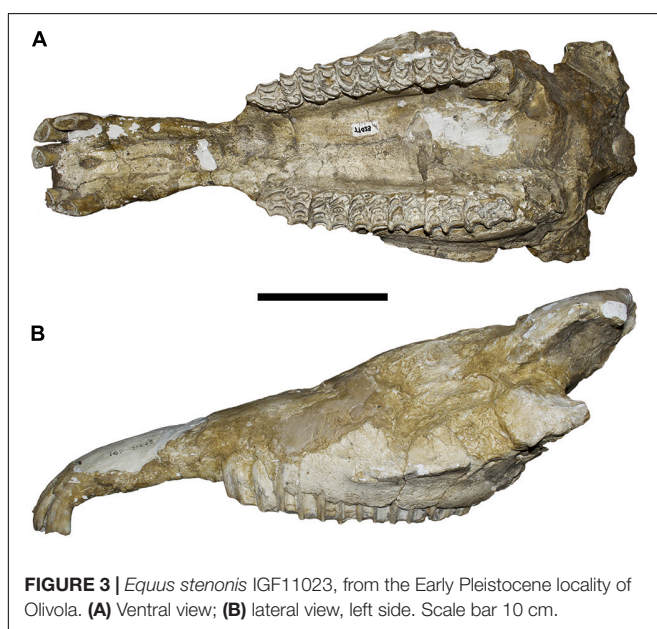

FIGURE 3 | *Equus stenonis* IGF11023, from the Early Pleistocene locality of Olivola. **(A)** Ventral view; **(B)** lateral view, left side. Scale bar 10 cm.

MATERIALS AND METHODS

3D *Equus stenonis* Digital Models

The *Equus stenonis* 3D digital meshes used in the analysis, the holotype skull IGF560 and the two target specimens Dm 5/154.3/4.A4.5 and IGF 11023, were acquired using the structural light 3D Scanner Artec Eva and Artec Space Spider[1]. The accuracy of the Artec Eva is up to 0.1 mm, with a resolution of 0.5 mm. It is capable of capturing the object's texture with a 1.3 megapixel resolution, with a 3D reconstruction rate for real time fusion of up to 16 frames per second, and a data acquisition speed of 2 million points for each second of recording. It works with a flash bulb (not a laser) 3D light source. Artec Eva is designed to digitally acquire objects larger than 10 cm. Artec Space Spider has a the 3D point accuracy of up to 0.05 mm, with a 3D resolution of 0.1 mm. It is capable of capturing the object texture with a 1.3 megapixel resolution, with a 3D reconstruction rate for real time fusion up to 7.5 frames per second, and a data acquisition speed of 1 million points each second of recording. It works with blue LED 3D light source. The optimal object size to be acquired under Artec Space Spider is > 5 cm.

Due to different target specifications, we used both scanners to build the IGF560, Dm 5/154.3/4.A4.5 and IGF 11023 3D meshes. Each skull was scanned with Artec Eva obtaining 6 partial scans (3 for dorsal view and 3 for ventral view), to acquire the external surface geometry. The upper teeth row and the incisor teeth have been scanned with Artec Space Spider (2 scans for each upper incisor row and the incisive arch, along the labial and lingual sides). Through the definition of morphological landmarks, the 12 digital scans obtained with the two light structured scanners have been aligned and the mesh created by using Artec Studio 14 software[2]. The 3D models have been exported in the .obj format.

Equus stenonis Target Deformation Protocol

Digital reconstruction techniques are becoming very popular in paleontology, as they represent a powerful tool to analyze disarticulated and damaged fossil remains, and even to reconstruct missing parts (Benazzi et al., 2014; Cunningham et al., 2014; Profico et al., 2019a).

Here we designed a workflow that sequentially combines different analytical tools and algorithms to obtain a virtual restoration of the *Equus stenonis* holotype skull (IGF560) by using target specimens as a guide (all meshes have been decimated to 500,000 triangles).

The procedure includes three steps:

1. Perform the retrodeformation of the *Equus stenonis* holotype (IGF560) by using a bilateral landmark configuration.
2. Align the target specimens (the Georgian Dm 5/154.3/4.A4.5 and IGF11023 from Olivola) to each other in order to calculate a mean target shape.

3. Warp the retrodeformed holotype onto the mean target shape.

Retrodeformation aims to remove asymmetric alterations due to taphonomic processes by applying a set of corresponding bilateral landmarks. An effective retrodeformation protocol was recently implemented by Schlager et al. (2018) and is available in the R software environment as embedded in the Morpho R package (Schlager, 2017). Despite traditional approaches (Ogihara et al., 2006; Gunz et al., 2009; Ghosh et al., 2010), this algorithm computes a non-linear symmetrization method detecting multiple local affine deformations reducing the interpolation performed by TPS (Bookstein, 1989). This protocol works with bilateral landmarks. For each pair of landmarks, their centroid is computed. The algorithm works by minimizing the stretch required to orthogonalize each local frame. The retrodeformation algorithm is embedded in the *retroDeformMesh()* function of the Morpho package (Schlager, 2017). The function uses a triangular mesh representing a digital model of the holotype, a set of bilateral landmarks to be placed directly on it, and a two-column matrix defining the left and right landmark indices. We used the IGF560 3D mesh as the

initial surface with a set of 60 bilateral landmarks (**Figure 4**). The landmarks are listed in **Supplementary Table S1**. All landmarks were manually sampled using the Amira software (ver. 5.4.5 thermofisher.com/amira-avizo). The 60 bilateral landmarks describe the entire morphology of IGF560. We avoid the use of surface semi-landmarks because the specimen IGF560 exhibits cracks and other damage on its surface. The aim of the retrodeformation procedure is to restore the original symmetry of IGF560. At the end of the process we obtained the retrodeformed version, IGF560R, of the original holotype IGF560 (**Figure 5A**).

The second step involved the alignment of the two target specimens (Dmanisi Dm 5/154.3/4.A4.5 and Olivola specimen IGF11023) and the calculation of a mean shape which can be used as a guide for further deformation (**Figure 5B**). The alignment of the two specimens was performed by applying the Digital Tool for Alignment (DTA), recently developed by Profico et al. (2019a) in the R environment (R Core Team, 2013) and embedded in the Arothron package (Profico et al., 2020). DTA uses the shape information contained in a reference sample (or in a reference specimen) to find the best alignment fit for disarticulated regions of a damaged specimen. To achieve this, the DTA algorithm includes first a generalized Procrustes Analysis
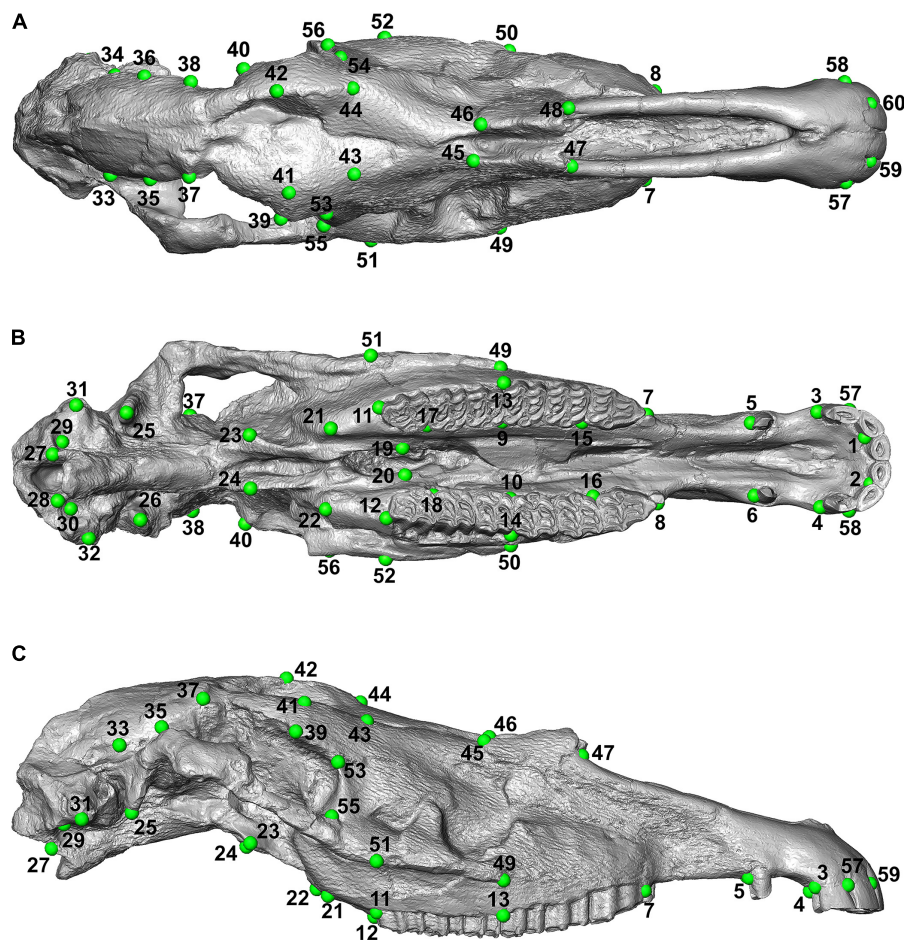

FIGURE 4 | Landmark configuration used on IGF560. **(A)** Dorsal view; **(B)** ventral view; **(C)** lateral view.
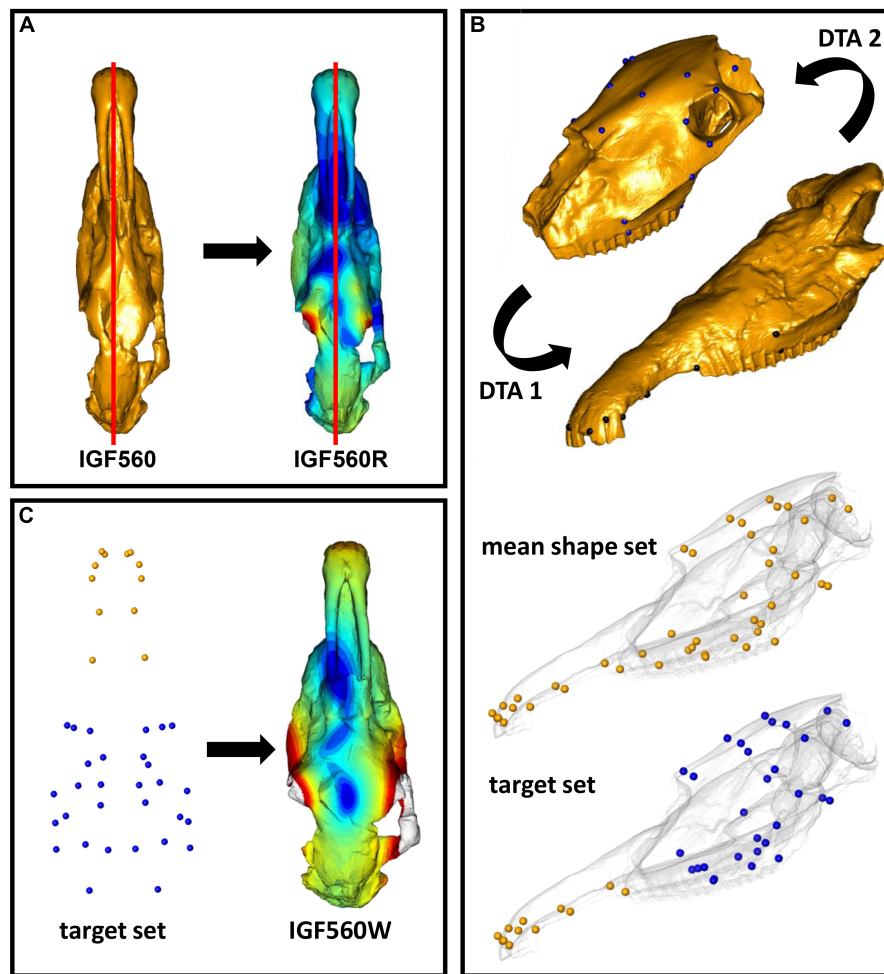
FIGURE 5 | Fossil restoration process explained step by step. **(A)** The IGF560 specimen is symmetrized by using *retroDeformMesh()* to obtain IGF560R. **(B)** IGF11023 is first oriented on Dm5 (DTA 1), then Dm5 is oriented on IGF11023 (DTA 2). A mean shape between the first aligned set and the second is computed. The target set is built by using the Dm5 landmark set and the landmarks of the mean shape set belonging to the snout. **(C)** IGF560R is warped via thin plate spline transformation based on the target configuration.

between the reference and target models. The quantification of the morphological distances between the aligned configuration and the reference model dataset allows us to choose the best reference model, identified in the alignment with the least morphological distance. In this case study, we performed two inverse DTAs (Dm5/154.3/4.A4.5 vs. IGF11023 and IGF11023 vs. Dm5/154.3/4.A4.5), by considering the two target specimens as if they were individually undeformed portions belonging to a single, disarticulated skull. We used a set of 30 bilateral landmarks for Dm 5/154.3/4.A4.5 and 24 bilateral landmarks for IGF11023 (**Figure 5B** and **Supplementary Table S1**). All landmarks were manually sampled with Amira software. Once we obtained two different aligned sets, we computed the mean shape.

Eventually, the third step consisted of warping IGF560R on the mean shape obtained by using the two targets. As we know that the Dm 5/154.3/4.A4.5 specimen is mostly undeformed, we decided to build the target set for the final warping by keeping all the landmarks originally sampled on

Dm 5/154.3/4.A4.5 and embedding all the extra landmarks coordinates from the mean shape set. The warping process was performed through the Morpho function *tps3d()* (Schlager, 2017), which deforms a set of coordinates or a mesh via thin plate spline transformation based on a reference and a target configuration. This step produced the retrodeformed and warped-to-targets mesh IGF560W (**Figure 5C**).

We further applied 3D reflection to IGF560R to obtain a perfectly symmetrical model with two zygomatic arches. This produces a symmetrical rendering of IGF560 which we refer to as IGF560R-S. We repeated the warping process on IGF560R-S, producing the virtual reconstruction IGF560W-S. The goal of the mirroring process is to compare the simple restoration procedure, as accomplished in IGF560R, to a more stretched application, where the starting digital model is forced to be symmetrical.

In order to compare the restoration model results, we used the Morpho function *meshDist()* (Schlager, 2017) to

compute the surface mesh distances between all the virtual models sharing the same mesh, that is all the pairwise comparisons between IGF560, IGF560R, IGF560W and their symmetrical equivalents IGF560R-S and IGF560W-S. The surface distances were computed as the differences between homologous vertex coordinates of two meshes, which can be retrieved by the Morpho function *vert2points()* (Schlager, 2017).

In addition, to visualize the local deformation between the original and the retrodeformed model we used the function *localmeshDist()* (Profico et al., 2020). The *localmeshDist* returns a 3D color map showing the local deformation in terms of area reduction or expansion. In this way, it is possible to visualize which areas during the target deformation procedure were either reduced or expanded.

Finally, we performed a Principal Component Analysis (PCA) by comparing biometric distances taken on the virtual specimens to equivalent measurements taken on several skulls of fossil and extant species to evaluate the goodness of the Target Deformation procedure.

TARGET DEFORMATION RESULTS

The Target Deformation results on the *Equus stenonis* holotype are shown in **Figure 6**. **Figures 6A–D** represent IGF560, IGF560R, IGF560W, respectively, with the color scale bar obtained from the *meshDist()* and *localmeshDist()* function to evaluate the morphological distance between the three target deformation versions of IGF560 (**Table 1**).

Compared to IGF560, IGF560R displays a maximal deformation of 12 mm in correspondence to the frontal bones above the orbital processes and the temporal bones, where the brain case has been rendered symmetrical on the right side. The left maxillary and premaxillary process, within the P^2-M^3 cheek teeth row, show a higher value of distance, due to the slight rotation on the left side of the original holotype. In ventral view, IGF560R renders the two upper teeth rows completely parallel. The palatine processes of the muzzle still remain medio-laterally compressed, even if the anterior breadth of the muzzle within the incisor arch (left I^3 – right I^3) displays a slight rotation on the right side. The palate exhibits a medium deformation between the two upper teeth rows, more evident on the left side.

FIGURE 6 | Comparison of the 3D models obtained with the Target Deformation. **(A)** Represent IGF560. Color gradient (from blue to red) indicates the increase in mesh vertex displacement in millimeters in IGF560R **(B)** and IGF560W **(C)**. Panel **(D)** shows the mesh triangles area variation in terms of contraction (red/yellow) and expansion (blue/purple).
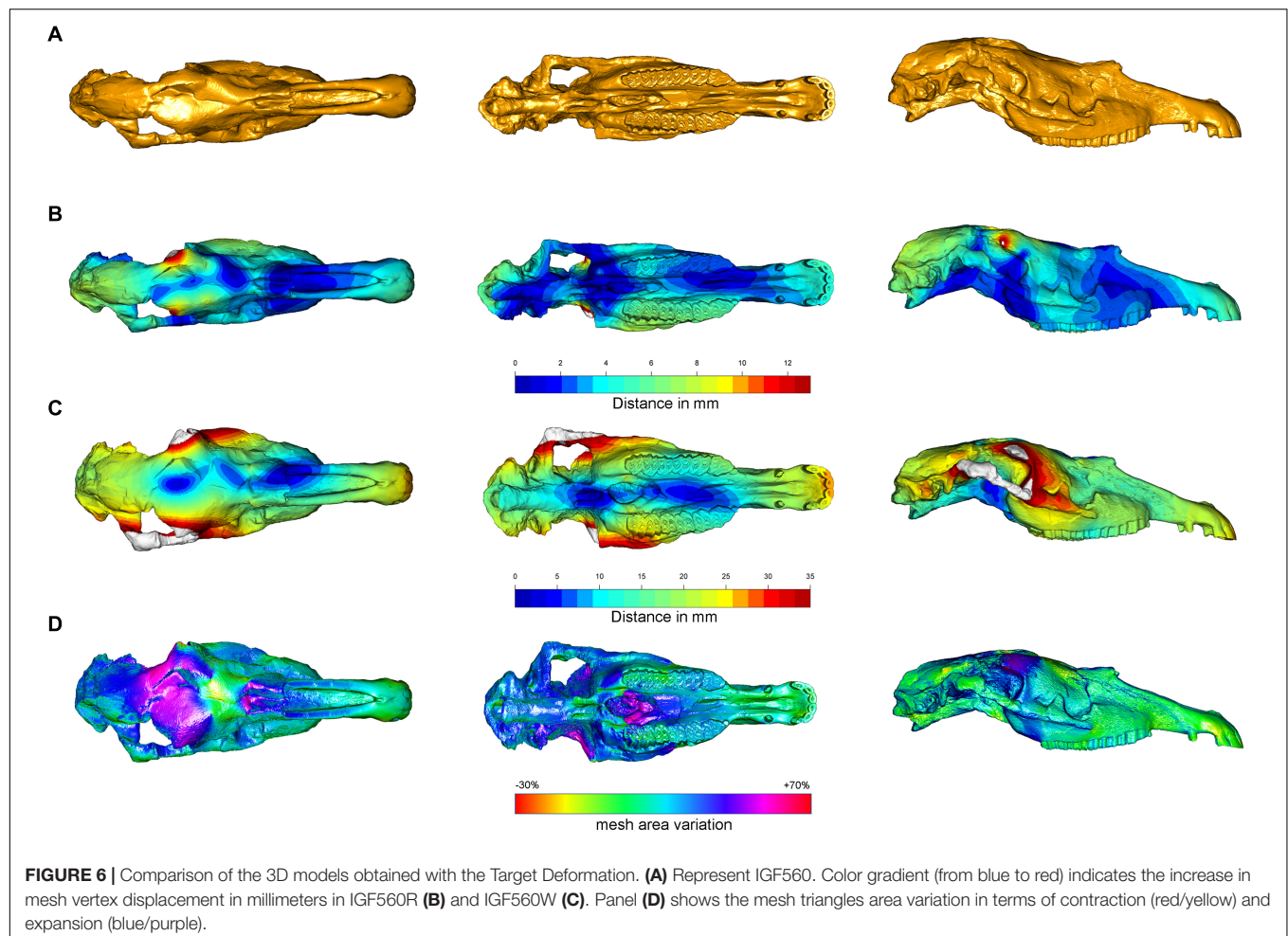
TABLE 1 | Surface mesh pairwise distances in terms of maximum (lower triangle) and absolute mean values (upper triangle) between IGF560, IGF560R, IGF560W, and their symmetrical equivalents IGF560R-S and IGF560W-S.

	Original model				Specular model	
	IGF560	**IGF560R**	**IGF560W**		**IGF560R-S**	**IGF560W-S**
IGF560	–	3.732	18.262	IGF560R-S	–	17.549
IGF560R	17.188	–	17.574	IGF560W-S	46.554	–
IGF560W	53.986	46.352	–			

Figure 6C renders a 3D model, IGF560, rendered by applying the DTA and tps3d protocols. Here, the power of Target Deformation becomes evident. This specimen exhibits an strong deformation on the right zygomatic arch, on both lateral facial crests behind the maxilla level and the orbits. The maximum distortion reached on this model is of 35 mm, as represented by the red areas. The temporal and occipital bones show the homologous deformation target, within a deformation average from 15 mm from the sagittal plane of the skull to 25 mm on both lateral sides. In ventral view, the best evidence of the Target Deformation is provided on the palate and the palatine process of the muzzle. The maximum palate distance between P^4 and M^1 is up to 28 mm, and between the posterior border of I^3 (see M13–M14–M15 in **Table 2**). It is remarkable that the two upper cheek teeth rows and maxilla processes behind the M^3 have not been broadened, and the upper teeth occlusal morphology has not been deformed. The choanae show the analogous deformation on both sides, within the sphenoid, the two paracondylar processes and occipital condyle. In ventral and lateral views, the muzzle and the nasal processes have been slightly elongated and widened, even if the final breadth of the palatine process does not diverge significantly from the holotype. This demonstrates that the maximum medio-lateral deformation has been reached in the central and posterior areas of the skull, whereas the muzzle has not been involved with the same stress deformation.

Supplementary Figure S1 illustrates the IGF560R-S model. To obtain this model, the right side of *Equus stenonis* Holotype has been reflected, to get a perfectly symmetrical skull with two zygomatic arches. In IGF560R-S, the damage on the left side of the holotype has been altered by restoring the left zygomatic arch. The Target Deformation performed on IGF560R-S has yielded IGF560W-S (**Supplementary Figure S1**). The results on this model are quite similar to IGF560W, with the most deformed areas represented from the two zygomatic arches, both lateral facial crests behind the maxilla level and the orbits. In ventral view, both sides of the skull exhibit a homologous level of deformation at the posterior borders of the I^3, in the palatine process and the palate and on the basal occipital region with sphenoid, the two paracondylar processes and occipital condyle. Greater deformation occurs on the upper incisors, probably due to a slight elongation of the muzzle. Deformation in the same area is also evident on IGF560W. No landmarks have been selected on the zygomatic arch (**Figure 4**), due to its absence on the left side of the holotype and also due to the incomplete preservation of both sides on the skull from Dmanisi. However, the results are in accordance with skull retrodeformation, even if slightly

TABLE 2 | Measurements of IGF560, IGF560W, IGF560R-S, and IGF560W-S. Measurements follow Eisenmann et al. (1988) and Bernor et al. (1997).

Specimen	IGF 560 Holotype	IGF 560W	IGF 560R-S	IGF 560W-S
M1	152.7	156.7	152.7	156.9
M2	122.6	128.8	120.8	130.3
M3	132.3	131.7	128.7	132.8
M4	148.1	145.9	152.5	147.6
M5	272.6	277.4	278.3	277.9
M6	540.8	550.3	537.8	550.9
M7	99.1	101.9	98.9	101.9
M8	82.5	81.9	81.7	81.6
M9	178.2	180.8	175.2	180.8
M10	97.5		90.3	
M11	17.8	34.3	19.2	31.9
M12	18.9	38.7	28.8	38.9
M13	50.9	78.8	51.8	78.6
M14	32.9	40.9	36.1	42.1
M15	62.8	69.9	64.3	68.7
M16	79.4	78.7	79.5	76.3
M17	171.8	165.7	168.3	165.4
M18	108.2	200.2	117.3	201.3
M19			160.4	234.6
M20			64.4	87.8
M21	89.2	105.5	98.3	107.1
M22	40.1		34.4	35.4
M23	407.5	439.8	406.7	436.5
M24	187.3	204.3	184.1	210.9
M25	114.8	115.3	117.6	115.8
M26	112.2	113.4	112.2	113.6
M27	12.8	12.3	11.9	12.3
M28	64.1	70.2	68.5	69.6
M29	45.6	53.4	47.1	54.8
M30	220.1	233.7	217.2	233.7
M31	166.6	165.9	163.1	169.4
M32	54.2	53.3	52.9	53.3
M33	75.5	77.9	73.1	77.8
M34	80.3	83.1	80.3	83.3
M35	28.4	28.1	28.4	28.4
M36	63.9	61.9	63.4	62.5
M37	65.6	60.7	65.6	61.3
M38	108.3	110.7	108.3	110.9

overestimated (see M19 in **Table 2**). Definitely, a set of control landmarks on the zygomatic arch and processes would have given a better result for this area of the skull.

The blue areas recognizable in dorsal view on IGF560W and IGF560W-S can be interpreted as the results of the original vector stress deformation to which IGF560 has been exposed. Indeed, these areas are located on the most damaged dorsal and ventral area of the skull and, in IGF560W, follow the deformation of the left side of the skull on the central region of the neurocranium.

In **Figure 6D** we reported the mesh area variations between IGF560 and IGF560W computed by using the function *localmeshDist*. Cold and warm color palettes indicate respectively local expansion and reduction in the final virtual reconstruction (i.e., IGF560W) compared to the original model (i.e., IGF560). The target deformation procedure leads to a great expansion of the neurocranium, which is laterally compressed and broken in the original specimen, and a moderate expansion of the ventral aspect of the right zygomatic arch. The choanae and the sphenoidal region show an analogous expansion on both sides. Only the upper portion of the frontal bone resulted in a contraction. The remaining anatomical regions of the IGF560 do not result in local differences.

MORPHOMETRIC ANALYSIS

We evaluated the Target Deformation performance by undertaking a PCA on the IGF560W and IGF560W-S models in addition to a set of fossil and extant *Equus* specimens. The skull measurements we used follow the standards published by Eisenmann et al. (1988) and Bernor et al. (1997). The comparison sample includes *Equus simplicidens* (Hagerman Horse Quarry, Idaho, United States, 3.3 Ma; Rook et al., 2019), *Equus eisenmannae* (Longdan, Linxia Basin, Gansu Province, China, 2.55 Ma; Wang and Deng, 2011; Rook et al., 2019), *Equus huanghoensis* (China, Early Pleistocene; Li et al., 2016; Sun and Deng, 2019), *Equus sanmeniensis* (China, Early Pleistocene; Sun and Deng, 2019), *Equus* sp. from Senèze (Senèze, France, 2.1 Ma; Nomade et al., 2014; Eisenmann, 2017), *Equus stenonis vireti* (Saint Vallier, France, 2.4 Ma; Nomade et al., 2014), *Equus koobiforensis* (Koobi Fora, Kenya, 1.9 Ma; Rook et al., 2019), and extant *Equus grevyi*. The IGF560 holotype has not been included in this sample due its severe medio-lateral deformation.

We have chosen the most distinctive skull measurements to evaluate whether IGF 560W and IGF 560W_S effectively place close to other *E. stenonis* specimens: M1 = basal length of the muzzle; M3 = vomerine length; M4 = post vomerine length: from the middle of the vomerine notch to basion; M6 = total basal length of the skull; M7 = upper premolar row length (P^2–P^4); M8 = upper molar row length (M^1–M^3); M9 = upper cheek tooth row length (P^2–M^3); M15 = muzzle width, between the posterior sides to distal limits of the I^3; M18 = frontal breadth behind the orbits; M23 = anterior ocular line: from the prosthion to the most external point of the orbital process; M30 = length of the naso-incisival notch: from the prosthion to the back of the narial opening; M31 = cheek length: from the back of the narial opening to the most anterior point of the orbit. The complete dataset used in the PCA is reported in **Supplementary Table S2**.

In **Figure 7** we reported the PCA plot showing the morphological similarities of IGF560W and IGF560W-S as compared to the comparative sample. The loadings of the PCA are reported in **Supplementary Figure S2**, whereas the PCA component values are shown in **Table 3**. The PC1 and PC2 explain the 59.4% of the total variance (PC1 = 36.89%; PC2 = 22.51%). PC1 mostly clusters specimens by the measurement M6 and M23 (total linear length) from negative to positive values. PC2 separates species by the M3 and M31 variables at positive values, and M4 and M30 at negative values. The two models obtained with the new Target Deformation protocol, IGF560W and IGF560W-S, are positioned closed to the *E. stenonis vireti* sample from Saint Vallier and the *Equus* sp. from the Early Pleistocene of Senèze. These results allow us to confirm the performance of the Target Deformation, where the two IGF560W and IGF560W-S 3D models can be considered as coherent and trustworthy with the skull morphology of the European *E. stenonis* samples form Saint Vallier and Senèze. Only these two localities have provided complete slightly deformed or undeformed skulls, which can be considered in a multivariate analysis including several skull measurements.

DISCUSSION AND CONCLUSION

The new virtual reconstruction protocol, which includes recent implementations in digital restoration of fossil specimens as retrodeformation (Schlager et al., 2018), a digital tool for alignment (DTA, Profico et al., 2019b), and 3D thin plate spline transformation (tps3d) (Schlager, 2017), has been applied on a case study utilizing one of the most important type specimens in the evolution of Old World *Equus* during the Pleistocene, the *Equus stenonis* from the Upper Valdarno Basin, Italy. We have demonstrated that this 3D virtual reconstruction protocol is capable of virtually restoring a severely crushed specimen by using partially complete skull specimens, such as the fragmentary *E. stenonis* skulls from Olivola and Dmanisi. Fossil horses are often deformed in their skull, due to their long and slender morphology and the presence of several pneumatized paranasal sinuses which occur within the skull. Through Target Deformation, the original shape of the skulls can be restored in a detail that allows performing morphologic, morphometric and phylogenetic analyses.

The Target Deformation study undertaken on the *E. stenonis* holotype IGF560 has produced the 3D model IGF560W which has revealed a skull morphology congruent with other specimens ascribed to the same species. This reconstruction is further supported by a multivariate analysis of cranial measurements. Our results indicate that the new 3D meshes IGF560W and IGF560W-S have a skull whose shape falls within the intraspecific variability of the European *Equus stenonis* from the Early Pleistocene of Saint Vallier and Senèze.

One potential caveat is that Target Deformation cannot provide shapes outside the range of the target specimens, potentially replicating their measurements. However, we argue that by producing intermediate shapes using separate specimens via DTA, Target Deformation does not produce measurement pseudoreplication, provided the original specimens are not themselves part of the analysis. In our case, neither the
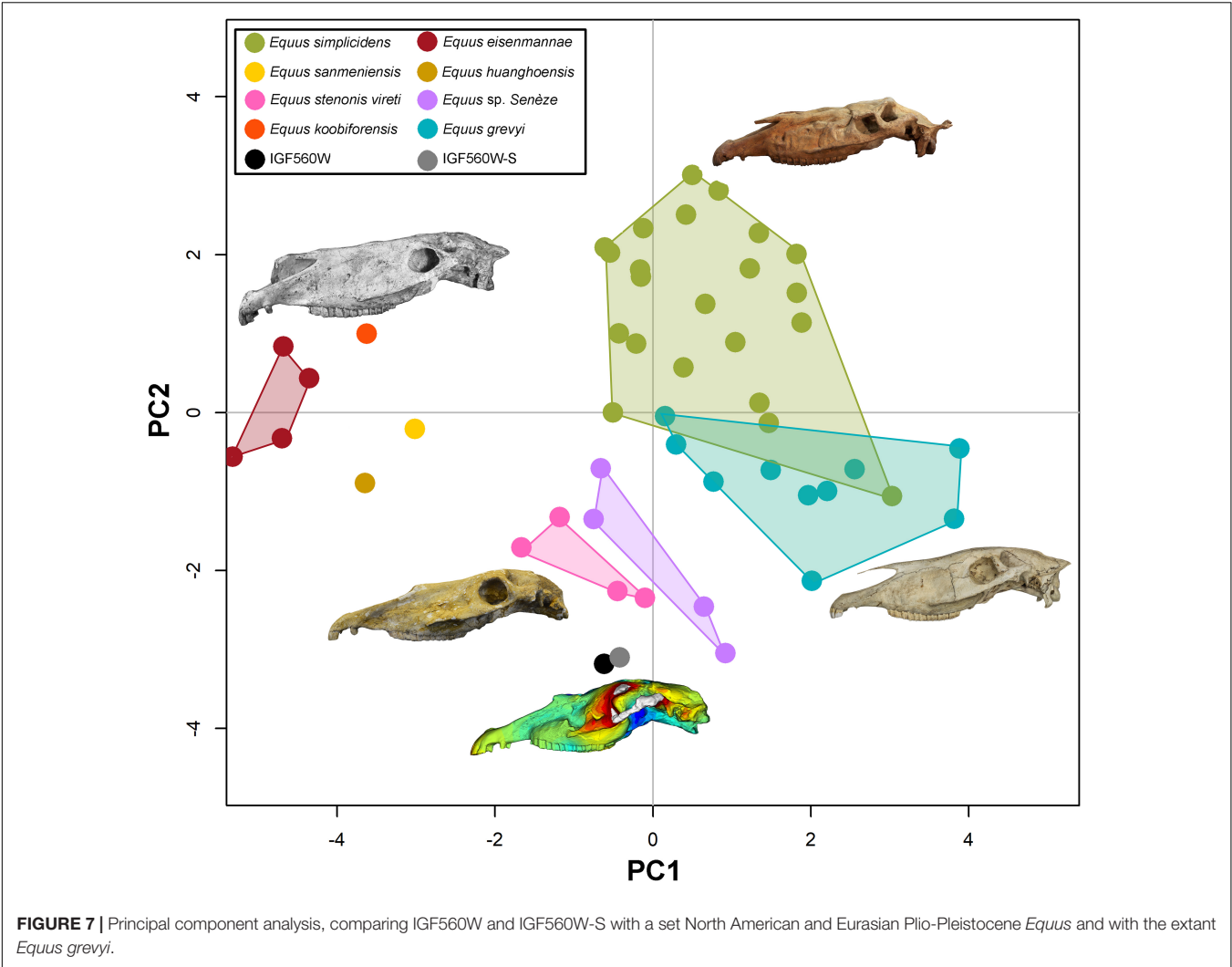
FIGURE 7 | Principal component analysis, comparing IGF560W and IGF560W-S with a set North American and Eurasian Plio-Pleistocene *Equus* and with the extant *Equus grevyi*.

TABLE 3 | PCA components values.

Importance of components	PC1	PC2	PC3	PC4	PC5	PC6
Standard deviation	2.1040	1.6434	1.2623	0.98985	0.91467	0.68406
Proportion of variance	0.3689	0.2251	0.1328	0.08165	0.06972	0.03899
Cumulative proportion	0.3689	0.594	0.7268	0.80843	0.87814	0.91714
Importance of components	**PC7**	**PC8**	**PC9**	**PC10**	**PC11**	**PC12**
Standard deviation	0.53857	0.48271	0.4559	0.36043	0.32237	0.17198
Proportion of variance	0.02417	0.01942	0.01732	0.01083	0.00866	0.00246
Cumulative proportion	0.94131	0.96073	0.97805	0.98887	0.99754	1.00000

incomplete Dmanisi and Olivola skulls, nor the mediolaterally compressed and partially broken IGF560 could serve the goal to perform a comparative analysis of *Equus* skull shape variation. Nevertheless, as reported in the PCA, the new 3D models obtained with the Target Deformation protocol, IGF560W and IGF560W-S, can be included in a morphometric multivariate analysis in order to increase the *E. stenonis* fossil skull representatives. This means target deformation promises to increase the statistical power of comparative analyses and could improve the digital restoration process. Although not specifically tested here, we argue that by sizing up deformation directly from the original specimens, Target Deformation can be a viable tool to study the impact of taphonomic distortion on fossil preservation.

The virtual restoration protocol presented here can be undertaken on any other 3D species model involving either

vertebrate or invertebrate fossils. Target Deformation could provide substantial improvement for examining and reporting damaged fossil specimens.

DATA AVAILABILITY STATEMENT

All datasets generated for this study are included in the article/**Supplementary Material**.

AUTHOR CONTRIBUTIONS

OC, MM, LR, and PR conceived the study. OC, MM, AP, and CS performed the analyses. All authors contributed to the article and approved the submitted version.

FUNDING

ACKNOWLEDGMENTS

SUPPLEMENTARY MATERIAL

The Supplementary Material for this article can be found online at: https://www.frontiersin.org/articles/10.3389/feart.2020.00247/full#supplementary-material

The external Supplementary Material for reproduction of the Target Deformation protocol (code and example data) are available on Zenodo: doi: 10.5281/zenodo.3895217.

FIGURE S1 | IGF560R-S **(A)** and IGF560W-S **(B)** comparison by *meshdist()*; color gradient (from blue to red) indicates the increase in mesh vertex displacement in millimeters.

FIGURE S2 | Principal component analysis loadings.

TABLE S1 | List of the selected landmarks on *Equus stenonis* IGF560 3D model.

TABLE S2 | Raw data used in the principal component analysis.

REFERENCES

Alberdi, M. T., and Palombo, M. R. (2013). The late early to early middle pleistocene stenonoid horses from Italy. *Quat. Int.* 288, 25–44. doi: 10.1016/j.quaint.2011.12.005

Alberdi, M. T., Ortiz Jaureguizar, E., and Prado, J. L. (1998). A quantitative review of European stenonoid horses. *J. of Paleontol.* 72, 371–387. doi: 10.1017/S0022336000036350

Athanassiou, A. (2001). New data on the *Equus stenonis* Cocchi, 1867 from the late pliocene locality of Sésklo (Thessaly. Greece). *Geodiversitas* 23, 439–469.

Azzaroli, A. (1964). The two villafranchian horses of the upper valdarno. *Palaeontogr. Ital.* 59, 1–12.

Azzaroli, A. (2003). Phylogeny of the genus *Equus* L. *Palaeontogr. Ital.* 84, 11–16.

Benazzi, S., Gruppioni, G., Strait, D. S., and Hublin, J. J. (2014). Virtual reconstruction of KNM-ER 1813 *Homo habilis* cranium. *Am. J. Phys. Anthropol.* 153, 154–160. doi: 10.1002/ajpa.22376

Bernor, R. L., Cirilli, O., Jukar, A. M., Potts, R., Buskianidze, M., and Rook, L. (2019). Evolution of Early *Equus* in Italy, georgia, the Indian subcontinent, East Africa, and the Origins of African Zebras. *Front. Ecol. Evol.* 7:166. doi: 10.3389/fevo.2019.00166

Bernor, R. L., Tobien, H., Hayek, L. A. C., and Mittmann, H. W. (1997). *Hippotherium primigenium* (*Equidae, Mammalia*) from the late Miocene of Höwenegg (Hegau, Germany). *Andrias* 10, 1–230.

Bookstein, F. L. (1989). Principal warps: thin-plate splines and the decomposition of deformations. *IEEE Trans. Pattern Anal. Mach. Intell.* 11, 567–585. doi: 10.1109/34.24792

Boulbes, N., and van Asperen, E. N. (2019). Biostratigraphy and Palaeoecology of European *Equus*. *Front. Ecol.Evol.* 7:301. doi: 10.3389/fevo.2019.00301

Budras, K. D., Sack, W. O., and Röck, S. (2009). *Anatomy of the Horse*. Hannover: Schlutersche Verkagsgesellscheft mbH & Co. KG.

Cocchi, I. (1867). L'uomo fossile dell'Italia Centrale (The fossil man in central Italy). *Memorie della Società Italiana Scienze Naturali* 2, 1–180.

Cunningham, J. A., Rahman, I. A., Lautenschlager, S., Rayfield, E. J., and Donoghue, P. C. (2014). A virtual world of paleontology. *Trends Ecol. Evol.* 29, 347–357. doi: 10.1016/j.tree.2014.04.004

De Giuli, C. (1972). On the type form of *Equus stenonis* Cocchi. *Palaeontogr. Ital.* 68, 35–49.

Eisenmann, V. (2017). *The Senèze equids*. Available online at: https://vera-eisenmann.com/the-seneze-equids-text (accessed December 5, 2020).

Eisenmann, V., Alberdi, M. T., De Giuli, C., and Staesche, U. (1988). "Studying Fossil Horses. Volume I – Methodology," in *Proceeding of the Collected papers after the New York International Hipparion Conference*, eds M. O. Woodburne and P. Y. Sondaar (Leiden: Brill), 1–71.

Forsten, A. (1999). A review of *Equus stenonis* Cocchi (*Perissodactyla, Equidae*) and related forms. *Quat. Sci. Rev.* 18, 1373–1408. doi: 10.1016/S0277-3791(98)00073-70

Forsyth Major, C. J. (1885). On the mammalian fauna of the Val d'Arno. *Quart. J. Geol. Soc. London* 41, 1–8. doi: 10.1144/GSL.JGS.1885.041.01-04.2

Ghosh, D., Amenta, N., and Kazhdan, M. (2010). *Closed form Blending of Local Symmetries*. Hoboken, NJ: Wiley Online Library, 1681–1688.

Gunz, P., Mitteroecker, P., Neubauer, S., Weber, G. W., and Bookstein, F. L. (2009). Principles for the virtual reconstruction of hominin crania. *J. Hum. Evol.* 57, 48–62. doi: 10.1016/j.jhevol.2009.04.004

Li, Y., Zhang, Y., Sun, B., Ao, H., and Xue, X. (2016). New fossils of the early pleistocene *Equus huanghoensis* (*Equidae, Perissodactyla*) from nihewan in hebei province of China. *Sci. China Earth Sci.* 59, 83–94. doi: 10.1007/s11430-015-5138-y

Lyman, R. L. (1994). *Vertebrate Taphonomy*. Cambridge: Cambridge University Press.

Nomade, S., Pastre, J. F., Guillou, H., Faure, M., Guérin, C., Delson, E., et al. (2014). Ar-40/Ar-39 constraints on some french landmark late pleistocene to early pleistocene large mammalian paleofaunas: paleoenviromental and paleoecological implications. *Quat. Geochronol.* 21, 2–15. doi: 10.1016/j.quageo.2012.12.006

Ogihara, N., Nakatsukasa, M., Nakano, Y., and Ishida, H. (2006). Computerized restoration of nonhomogeneous deformation of a fossil cranium based on bilateral symmetry. *Am. J. Phys. Anthropol.* 130, 1–9. doi: 10.1002/ajpa.20332

Palombo, M. R., Alberdi, M. T., Bellucci, L., and Sardella, R. (2017). An intriguing middle-sized horse from coste san giacomo (Anagni Basin, central Italy). *Q. Res.* 87, 347–362. doi: 10.1017/qua.2017.6

Palombo, M. R., and Alberdi, M. T. (2017). Light and shadows in the evolution of South European stenonoid horses. *Fossil. Imprint* 73, 115–140. doi: 10.2478/if-2017-0006

Prat, F. (1964). Contribution a la classification des equidés villafranchiens. *Procès Verbaux de la Société Linnéenne de Bordeaux* 101, 14–32.

Profico, A., Bellucci, L., Buzi, C., Di Vincenzo, F., Micarelli, I., Strani, F., et al. (2019a). Virtual anthropology and its application in cultural heritage studies. *Stud. Conserv.* 64, 323–336. doi: 10.1080/00393630.2018.1507705

Profico, A., Buzi, C., Davis, C., Melchionna, M., Veneziano, A., Raia, P., et al. (2019b). A new tool for digital alignment in virtual anthropology. *Anat. Rec.* 302, 1104–1115. doi: 10.1002/ar.24077

Profico, A., Buzi, C., Melchionna, M., Piras, P., Raia, P., and Veneziano, A. (2020). *Arothron: Geometric Morphometrics Analysis and Virtual Anthropology. R package version 1.1.1.*

R Core Team (2013). *R: A Language and Environment for Statistical Computing.* Vienna: R Core Team.

Rook, L., Bernor, R. L., Avilla, L. D., Cirilli, O., Flynn, L., Jukar, A. M., et al. (2019). Mammal biochronology (Land mammal ages) around the world from the late miocene to middle pleistocene and major events in horse evolutionary history. *Front. Ecol. Evol.* 7:278. doi: 10.3389/fevo.2019.00278

Schlager, S. (2017). "Morpho and Rvcg - shape analysis in R," in *Statistical Shape and Deformation Analysis*, eds G. Zheng, S. Li, and G. Szekely

(Cambridge: Academic Press), 217–256. doi: 10.1016/b978-0-12-810493-4.00011-0

Schlager, S., Profico, A., Di Vincenzo, F., and Manzi, G. (2018). Retrodeformation of fossil specimens based in 3D bilateral semi-landmarks: implementation in the R package "Morpho". *PLoS One* 13:e0194073. doi: 10.1371/journal.pone.0194073

Shipman, P. (1981). *Life History of a Fossil and Introduction to Taphonomy and Paleoecology.* Cambridge: Harvard University Press.

Sun, B., and Deng, T. (2019). The *Equus* datum and the early radiation of *Equus* in China. *Front. Ecol. Evol.* 7:429. doi: 10.3389/fevo.2019.00429

Vekua, A. (1995). Die wirbeltierfauna des villafranchian von dmanisi und ihre biostratigraphisce bedeutung. *Jb. Röm. Ger. ZentMus. Mainz* 42, 77–180.

Wang, S.-Q., and Deng, T. (2011). Some evolutionary trends of *Equus eisenmannae* (Mammalia, Perissodactyla) in the stratigraphic sequence of Longdan, China, in comparison to modern *Equus*. *J. Vertebr. Paleontol.* 31, 1356–1365. doi: 10.1080/02724634.2011.611203